Received: 16 March 2023 | Revised: 13 July 2023 | Accepted: 21 July 2023

DOI: 10.1002/glia.24450

GLIA

WILEY

RESEARCH ARTICLE

Increased membrane Ca^{2+} permeability drives astrocytic Ca^{2+} dynamics during neuronal stimulation at excitatory synapses

Jarand B. Hjukse[1] | Mario F. D. L. Puebla[1,2,3] | Gry Fluge Vindedal[1] | Rolf Sprengel[4] | Vidar Jensen[1] | Erlend A. Nagelhus[1,5†] | Wannan Tang[1,2,3]

[1]Department of Molecular Medicine, Institute of Basic Medical Sciences, University of Oslo, Oslo, Norway

[2]Department of Clinical and Molecular Medicine, Norwegian University of Science and Technology (NTNU), Trondheim, Norway

[3]Department of Neurology, Neuroclinic, St. Olavs Hospital, Trondheim, Norway

[4]Department of Neurology, Oslo University Hospital, Oslo, Norway

[5]Research Group of Molecular Neurobiology, Max Planck Institute for Medical Research, Heidelberg, Germany

Correspondence
Vidar Jensen, Department of Molecular Medicine, Institute of Basic Medical Sciences, University of Oslo, Oslo 0372, Norway.
Email: vidar.jensen@medisin.uio.no

Wannan Tang, Department of Clinical and Molecular Medicine, Norwegian Universtity of Science and Technology (NTNU), Trondheim, 7491, Norway.
Email: wannan.tang@ntnu.no

Funding information
European Union's Seventh Framework Programme for Research, Technological Development and Demonstration, Grant/Award Number: 601055; Felles Forskningsutvalg (FFU), Grant/Award Number: 34226; HELSE MIDT-NORGE, Grant/Award Number: 28293; Letten Foundation; The Research Council of Norway, Grant/Award Number: 262552

Abstract

Astrocytes are intricately involved in the activity of neural circuits; however, their basic physiology of interacting with nearby neurons is not well established. Using two-photon imaging of neurons and astrocytes during higher frequency stimulation of hippocampal CA3-CA1 Schaffer collateral (Scc) excitatory synapses, we could show that increasing levels of released glutamate accelerated local astrocytic Ca^{2+} elevation. However, blockage of glutamate transporters did not abolish this astrocytic Ca^{2+} response, suggesting that astrocytic Ca^{2+} elevation is indirectly associated with an uptake of extracellular glutamate. However, during the astrocytic glutamate uptake, the Na^{+}/Ca^{2+} exchanger (NCX) reverse mode was activated, and mediated extracellular Ca^{2+} entry, thereby triggering the internal release of Ca^{2+}. In addition, extracellular Ca^{2+} entry via membrane P2X receptors further facilitated astrocytic Ca^{2+} elevation via ATP binding. These findings suggest a novel mechanism of activity induced Ca^{2+} permeability increases of astrocytic membranes, which drives astrocytic responses during neuronal stimulation of CA3-CA1 Scc excitatory synapses.

KEYWORDS
astrocytes, Ca^{2+} signals, glutamate transporter, IP3R2 receptor, membrane Ca^{2+} permeability, Na^{+}/Ca^{2+} exchanger (NCX), P2X receptor, two-photon imaging

1 | INTRODUCTION

Most recent neuroimaging technologies have revolutionized our knowledge on the function of astrocytes, the predominant glial cell type in the brain. However, mechanisms underlying neuronal stimulation evoked astrocytic Ca^{2+} signals are debated and vary between species, brain regions, developmental stages and astrocytic subcellular compartments (Deitmer & Rose, 2010; Doengi et al., 2009; Droste et al., 2017; Saab et al., 2012; Santello et al., 2019; Tang et al., 2015; Zhang et al., 2019). As important contributors to elicit astrocytic Ca^{2+} responses during

†Deceased.

neuronal stimulation, various neurotransmitters, ion channels, G-protein coupled receptors, and neurotransmitter transporters embedded in the astrocytic membrane are involved in this controversy (Bazargani & Attwell, 2016; Deitmer & Rose, 2010; Santello et al., 2019).

It has been long considered that metabotropic glutamate receptors (mGluRs) and P2 purinergic receptors are the main contributors for the neuronal stimulation evoked astrocytic Ca^{2+} signals (Bowser & Khakh, 2004; Porter & McCarthy, 1996). However, our previous study showed that the triple blockage of group I/II metabotropic glutamate receptors and P2 purinergic receptors causes only about a one third reduction of the Ca^{2+} elevation in both astrocytic somata and processes at the activated hippocampal CA3-CA1 Schaffer collateral (Scc) synapses of adult mice (Tang et al., 2015). This indicates other potential pathways that can trigger Ca^{2+} elevation in astrocytes during neuronal stimulation.

The basal level of the astrocytic intracellular Ca^{2+} at the resting state is tightly regulated at low concentrations (about 100 nM or below), which is necessary of maintaining astrocytic physiological functions (Deitmer & Rose, 2010; King et al., 2020; Shigetomi et al., 2010). Unlike neurons, fewer pathways allowing extracellular Ca^{2+} entry are present in astrocytic membranes, including receptors, channels, exchangers, and pumps. This leads to a highly restricted Ca^{2+} permeability of the astrocytic membrane (Bazargani & Attwell, 2016). However, whether neuronal stimulation evoked astrocytic Ca^{2+} elevation is associated with changes of this limited astrocytic membrane Ca^{2+} permeability has remained unclear.

Meanwhile, many studies have shown that the intracellular Na^+ homeostasis is a key property of maintaining the cellular function of astrocytes (Deitmer & Rose, 2010; Felix et al., 2020; Kirischuk et al., 2012; Rose & Karus, 2013a). Both locally restricted Na^+ concentration and global Na^+ transients in the complete territory of astrocytes may serve as important signals for varies astrocytic functions (Felix et al., 2020; Kirischuk et al., 2012; Rose & Karus, 2013a). At the excitatory synapses, glutamate uptake is one of the major pathways in astrocytes to initiate Na^+ signaling, and the amount of glutamate released from neurons can be translated into corresponding Na^+ transients in astrocytes via glutamate uptake (Deitmer & Rose, 2010; Rose et al., 2020; Rose & Karus, 2013a; Rose & Verkhratsky, 2016). This glutamate uptake is mediated by Na^+-dependent glutamate transporters GLAST (EAAT1) and/or GLT-1 (EAAT2). In addition, this mechanism is also one of the main factors for the clearance of extracellular glutamate in varies brain regions (Bennay et al., 2008; Bergles & Jahr, 1998; Kirischuk et al., 2007; Langer & Rose, 2009; Rose et al., 2020).

Closely associated with Na^+-dependent glutamate transporters, the Na^+/Ca^{2+}-exchanger (NCX) is an important membrane protein that operates either in its forward (Na^+ in) or reverse (Na^+ out) mode. It exchanges three Na^+ for one Ca^{2+} and its E_{rev} lies between −90 and −60 mV (Felix et al., 2020; Rose et al., 2020). In astrocytes, the NCX contributes to the maintenance of low intracellular Ca^{2+} levels with its forward mode (Bondarenko et al., 2005; Goldman et al., 1994; Kirischuk et al., 1997). However, moderate glutamate-induced Na^+ influx can cause reversal of the NCX and thereby induce Ca^{2+} signals (Rojas et al., 2007; Rose et al., 2020). This counteract of astrocytic Na^+ loads initiates Ca^{2+} entry from the extracellular space (Kirischuk et al., 2012). Furthermore, it has been reported in an *in vivo* mouse stroke model that increases of Na^+ induce a cortical astrocytic Ca^{2+} influx through the reverse mode of NCX (Gerkau et al., 2018).

By using various frequency protocols, we started with characterizing presynaptic glutamate releases during electrical stimulation of Scc synapses in acute mouse brain slices via a genetically encoded glutamate sensor iGluSnFR (Marvin et al., 2013). We then performed dual color two-photon imaging using genetically encode Ca^{2+} indicator (GECI) GCaMP6f and jRGECO1a in both astrocytes and neurons, respectively. We conclude that the increased astrocytic membrane Ca^{2+} permeability via NCX is of primary importance for triggering the local neuronal evoked Ca^{2+} elevation in astrocytes. In addition, the opening of P2X channels can further increase the astrocytic membrane Ca^{2+} permeability causing Ca^{2+} elevation in astrocytes.

2 | MATERIALS AND METHODS

2.1 | Animals

Both male and female wild type (C57BL6J, Janvier Labs) and *Itpr2*$^{-/-}$ (*Itpr2*$^{tm1.1Chen}$; MGI: 3640970) (Li et al., 2005) mice at least 6 weeks of age were housed with a 12-h light/dark cycle (light on at 8 a.m.). *Itpr2*$^{-/-}$ mice were backcrossed into a C57BL6J background for at least 15 generations. All experimental procedures were approved by the Norwegian Food Safety Authority (project number: FOTS 11255).

2.2 | Plasmid construction and virus production

The DNA sequences for the genetically encoded fluorescent Ca^{2+} indicator GCaMP6f (Chen et al., 2013) and jRGECO1a (Dana et al., 2016) were first amplified by PCR from pGP-CMV-GCaMP6f and pGP-CMV-NES-jRGECO1a (Addgene) with 5' BamHI and 3' HindIII, and sub-cloned into the recombinant adeno-associated virus (rAAV) vector pAAV-6P-SEWB (Shevtsova et al., 2005) for generating pAAV-*SYN*-GCaMP6f and pAAV-*SYN*-jRGECO1a, respectively. The human glial fibrillary acidic protein (*GFAP*) promoter (Hirrlinger et al., 2009) was inserted with MluI and BamHI into pAAV-*SYN*-GCaMP6f construct for obtaining pAAV-*GFAP*-GCaMP6f. Plasmid pAAV-*SYN*-iGluSnFR (Marvin et al., 2013) was used to express the genetically encoded fluorescent glutamate indicator iGluSnFR. Serotype 2/1 rAAVs from pAAV-*GFAP*-GCaMP6f, pAAV-*SYN*-jRGECO1a and pAAV-*SYN*-iGluSnFR were produced (Tang et al., 2015) and purified by AVB Sepharose affinity chromatography (Smith et al., 2009), following titration with real-time PCR (rAAV titer about 1.0–6.0 × 10^{12} viral genomes/mL, TaqMan Assay, Applied Biosystems). For hippocampal rAAV-transduction of both astrocytes and neurons, rAAV-*GFAP*-GCaMP6f and rAAV-*SYN*-jRGECO1a were mix 1:1.

2.3 | Surgical procedures and virus transduction

Viruses were stereotactically and bilaterally injected into brains of deeply anesthetized (mixture of zolazepam [188 mg/kg body weight],

tiletamine [188 mg/kg body weight], xylazine [4.5 mg/kg body weight] and fentanyl [26 μg/kg body weight]) 6–8-week-old C57BL6/J and *Itpr2*$^{-/-}$ mice (Janvier Labs) as described (Tang et al., 2015). For transduction in adult mouse hippocampi, stereotactic coordinates relative to Bregma were anteroposterior −2.0 mm, lateral ±1.5 mm. During injection, about 0.3 μL of purified rAAVs in total were delivered into each hippocampus with 1.5 mm in depth. All procedures were performed according to the guidelines of the local animal use and care committees.

2.4 | Electrophysiology and *ex vivo* two-photon Ca^{2+} imaging

Experiments were performed on acute hippocampal slices prepared from adult mice 2–6 weeks after rAAV transduction. The acute hippocampal slices were prepared as described (Tang et al., 2015) and kept at 30 ± 1°C. Two glass electrodes filled with ACSF and positioned 100–150 μm away from each other in CA1 *stratum radiatum* served as stimulation and recording electrodes (fEPSP monitoring), respectively. In iGluSnFR experiments, DL-2-Amino-5-phosphonopentanoic acid (APV, 50 μM, Tocris) was added to the ACSF to avoid the unintended N-methyl-D-aspartate receptor (NMDAR) dependent plasticity. In order to stimulate the approximate same number of axons in the iGluSnFR experiment, we adjusted the stimulation strength so that we could record a prevolley of 1.0 mV in amplitude. In the GCaMP6f experiment we adjusted the stimulation strength to just below thresholds for eliciting a population spike on the third fEPSP in a triple stimulation protocol (three stimulation pulses with 20 ms interstimulus interval). In some experiments chemical blockers DL-TBOA (100 μM, Tocris), KB-R7943 (20 μM, Tocris), and PPADS (100 μM, Tocris) were added into ACSF. Recordings were done both before the exposure to the drugs and 60 min post-exposure. Stimulation in trains (20 Hz for 10 sec, 20 Hz for 1 sec, or theta burst [five stimulation trains at 100 Hz repeated five times every 200 msec] were selectively applied during experiments). The GCaMP6f, jRGECO1a and iGluSnFR fluorescence were recorded by a two-photon laser scanning microscope (model "Ultima", Prairie Technologies) with a "XLPLN 25 × WMP" 1.05NA water-immersion objective (Olympus, Tokyo, Japan) at 900–910 nm (for imaging GCaMP6f and iGluSnFR) or 980–1020 nm (for dual-indicator imaging) laser pulse using a "Chameleon Vision II" (Coherent, Santa Clara, CA, USA) laser. Two-photon imaging was performed with 30 sec baselines followed by electrical stimulations. The recordings were done either with 1–5 Hz for low imaging sampling rate (512 × 512 px or 256 × 256 px), or 50 Hz for high imaging sampling rate (50 × 50 px, for iGluSnFR experiments).

2.5 | Imaging analysis

Calcium signals were extracted and analyzed in MATLAB, using the Begonia toolbox (Bjørnstad et al., 2021) (https://github.com/GliaLab/Begonia) and custom-made scripts. For the dual-indicator latency experiment, astrocyte regions of interest (ROIs) were manually drawn, distinguishing three compartments according to the morphology: Astrocyte Endfeet (AE), Astrocyte Processes (AP, at least 5 μm away from the perimeter of somata) and Astrocyte Somata (AS). The neuronal signals were calculated from the recorded *striatum rediatum* region selected as one complete ROI to include all neuronal terminals at once. In the iGluSnFR experiment, circular ROIs of 5 μm were placed. Relative fluorescence was calculated with the formula $\Delta F/F = (F_t - F_0)/F_0$, where F_t is the mean fluorescence intensity of the pixels inside each ROI at a given time, and F_0 is defined as the mode from the first 30 sec baseline period. Astrocyte calcium responses to Scc electrical stimulation (ES) were detected if calcium onsets occurred no later than 10 sec after the neuronal onset. Both onsets from astrocytes and neurons were defined as the moment when the signal reaches two times standard deviation (SD) value over the baseline after ES. This SD was calculated with values of 10th percentile of the first 30 sec baseline period before the ES. In addition to the manual ROI analysis, an automatic calcium signal analysis algorithm that detects regions of activity (ROA) in a pixel-by-pixel fashion, was used as described (Bjørnstad et al., 2021). The ROA implementation together with ROI increased the analysis sensitivity, as it outputs the percentage of active pixels of individual ROI / compartments instead of relative fluorescence changes. To illustrate the field $\Delta F/F$ and ROA, the recorded *striatum radiatum* regions were selected as one complete ROI in the analysis mentioned above.

2.6 | Statistical analysis

Statistical analyses were performed using Prism (Version 9.3.1 for Mac OSX, GraphPad Software). Full descriptions of statistical parameters were accessed with the original data before choosing the suitable analysis. Kruskal-Wallis test and Dunn's multiple comparison test were used for amplitudes with distances measurement of iGluSNF signals. Ordinary one-way ANOVA and Tukey's multiple comparison test were used for amplitude comparison of different stimulation protocols of iGluSnFR. Wilcoxon matched-pairs signed rank test was used for measurements of recovery rate of iGluSnFR fluorescence after first, last train during theta burst stimulation, the relative latency of dual-indictor measurement with protocols of 20 Hz for 1 sec and theta burst. Mann–Whitney test was performed for the latency of dual-indictor measurement with protocols of theta burst and 20 Hz for 10 sec. Paired t test was performed with the DL-TBOA experiment. Two-way ANOVA with multiple comparisons test (Sidak's multiple comparisons test) was performed with KB-R7943 and KB-R7943 + PPADS experiments, ACSF wash control and *Itpr2*$^{-/-}$ mice experiments.

3 | RESULTS

3.1 | Characterization of presynaptic glutamate releases with various neuronal stimulation at CA3-CA1 synapses

At hippocampal CA3-CA1 Scc fibers, glutamate is the main neurotransmitter released at excitatory synapses. Glutamate released from

local neuronal stimulation contributes to the increase of astrocytic intracellular Ca^{2+} as shown in our previous study (Tang et al., 2015). Before accessing potential cellular mechanisms related to astrocytic glutamate uptake triggering Ca^{2+} elevation in astrocytes, we first characterized presynaptic glutamate releases during neuronal stimulation with three incremental stimulation protocols (20 Hz for 1 sec, 20 Hz for 10 sec and theta burst for 1 sec with five trains at 100 Hz repeated five times every 200 msec). With respective neuronal stimulation, the released glutamate was measured by a genetically encoded fluorescent glutamate sensor iGluSnFR under *hSYN* promoter expressed with a rAAV vector (Marvin et al., 2013). Stimulation of Scc yielded a sharp increase in iGluSnFR fluorescence throughout the *stratum radiatum* (Figure 1a,b), albeit with various protocols and distances to the stimulating electrode (Figure 1b–h). Even during the highest frequency theta burst protocol, iGluSnFR transients did tightly accompany every stimulation train, with a recovery time of 40–50 msec (Figure 1g,i). Intriguingly, the theta burst protocol evoked an iGluSnFR fluorescence increase ($\Delta F/F$) of significant higher peak amplitudes than the other two protocols (Figure 1h). Particularly, when considering reported kinetics of iGluSnFR (rise time about 30 msec and decay time about 180 msec), the 1 sec theta burst stimulation may evoke more glutamate than 20 Hz for 1 sec protocol, suggesting that higher frequency stimulation results greater level of extracellular glutamate.

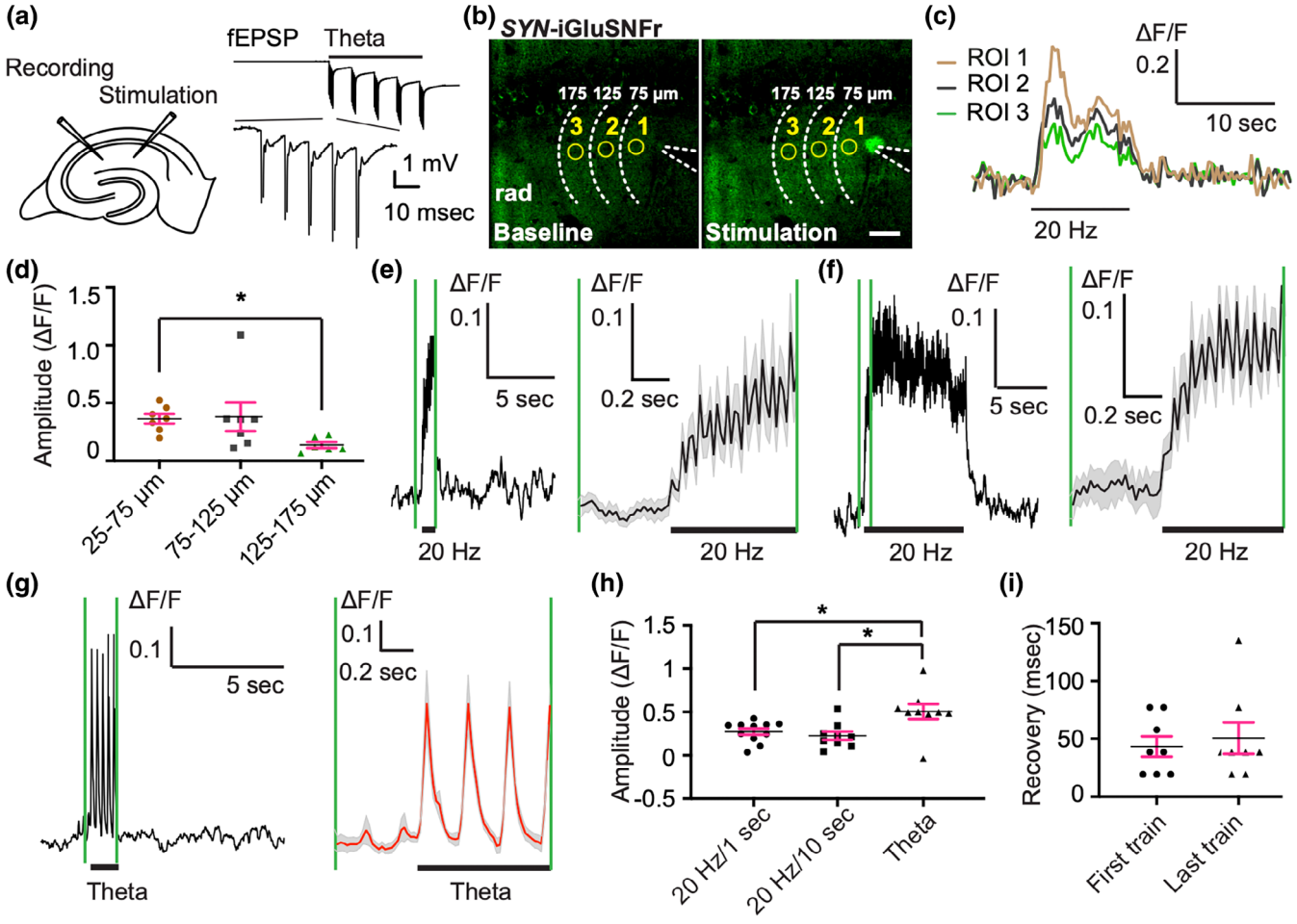

FIGURE 1 Neuronal stimulation evoked elevation of extracellular glutamate levels. (a) Left, schematic drawing of the electrode placement; right, representative trace of fEPSP (expanded in bottom trace) recorded during theta burst stimulations. (b) Images of *SYN*-iGluSnFr fluorescence in adult mouse hippocampus before (baseline) and after 20 Hz for 10 sec Scc stimulation. Dashed lines indicate position of the stimulation electrode and distance to the electrode tip. Scale bar, 50 µm. (c) Representative traces of three regions of interest (ROIs 1–3) indicated in the images of (b). Black bar indicates 20 Hz for 10 sec Scc stimulation. (d) Amplitude of stimulation evoked (20 Hz for 10 sec) extracellular iGluSnFr fluorescence at different distances from the stimulation electrode ($p = .0059$, $n_{25–75\ \mu m} = 7$, $n_{75–125\ \mu m} = 7$, $n_{125–175\ \mu m} = 6$). (g) Average traces of *SYN*-iGluSnFr fluorescence during neuronal stimulation (indicated with bars) at 20 Hz for 1 sec (e), at 20 Hz for 10 sec (f) and theta burst (G). Traces between the green vertical lines are expanded on the right side. Gray shades indicate the range of standard error mean. (h) Amplitudes of stimulation-evoked extracellular iGluSNFr fluorescence (ordinary one-way ANOVA, $p = .0059$, $F_{(2,26)} = 6.285$,$n_{20\ Hz\ for\ 1\ sec} = 9$,$n_{20\ Hz\ for\ 10\ sec} = 11$, $n_{Theta} = 9$; Tukey's multiple comparison test, $p_{20\ Hz\ for\ 1\ sec\ versus\ Theta} = .0080$, $p_{20\ Hz\ for\ 10\ sec\ versus\ Theta} = .0217$). (i) iGluSnFr fluorescence recovery rate of first and last train during theta burst stimulation ($p = .8750$, $n = 8$). Asterisks in (d) and (h) show values that differ significantly from each other. Pink bars in (d), (h), and (i) indicate the standard error mean.

3.2 | Simultaneous assessment of neuronal and astrocytic Ca^{2+} elevation at activated CA3-CA1 synapses

To further investigate the dynamics of astrocytic Ca^{2+} elevation in relation to the glutamate released from Scc synapses, we used wild-type mice transduced with a mixture of rAAV-*SYN*-jRGECO1a (Dana et al., 2016) and rAAV-*GFAP*-GCaMP6f (Enger et al., 2015) to simultaneously reveal neuronal and astrocytic Ca^{2+} signals, respectively. Both 20 Hz for 1 sec and theta burst stimulation of Scc (Figure 2a) evoked distinct increases in neuronal jRGECO1a (red) and astrocytic GCaMP6f (green) fluorescence ($\Delta F/F$, Figure 2b,c). We then performed both protocols on the same set of acute hippocampal slices one after another. To avoid potential changes of sample conditions that could influence astrocytic responses under strong stimulation protocols, the 20 Hz for 1 sec protocol was always performed prior to the theta burst protocol in the same acute slice. Here, we found that the relative latency of astrocytic Ca^{2+} elevation in all compartments (somata, processes and endfeet) occurred about 2.5 sec after the neuronal Ca^{2+} rise with 20 Hz for 1 sec stimulation protocol (Figure 2d). However, a significant shorter relative latency in astrocytic somata and processes (about 1.7 sec) was detected by using theta burst stimulation (Figure 2d), indicating that the higher frequency stimulation resulted in a faster onset of astrocytic Ca^{2+} elevation. Together with the above iGluSnFR experiment, we show that greater extracellular glutamate released from higher frequency stimulation of neurons accelerates local astrocytic Ca^{2+} elevation. We then further tested the 20 Hz for 10 sec protocol in a separate set of acute slices. Despite of significant lower glutamate peak amplitude found in above iGluSnFR experiment compared to theta burst simulation (Figure 1h), the relative latency in all astrocytic compartments were similar as the ones observed with theta burst stimulation (Figure 2d). This may be due to the accumulated greater level of total glutamate released during the

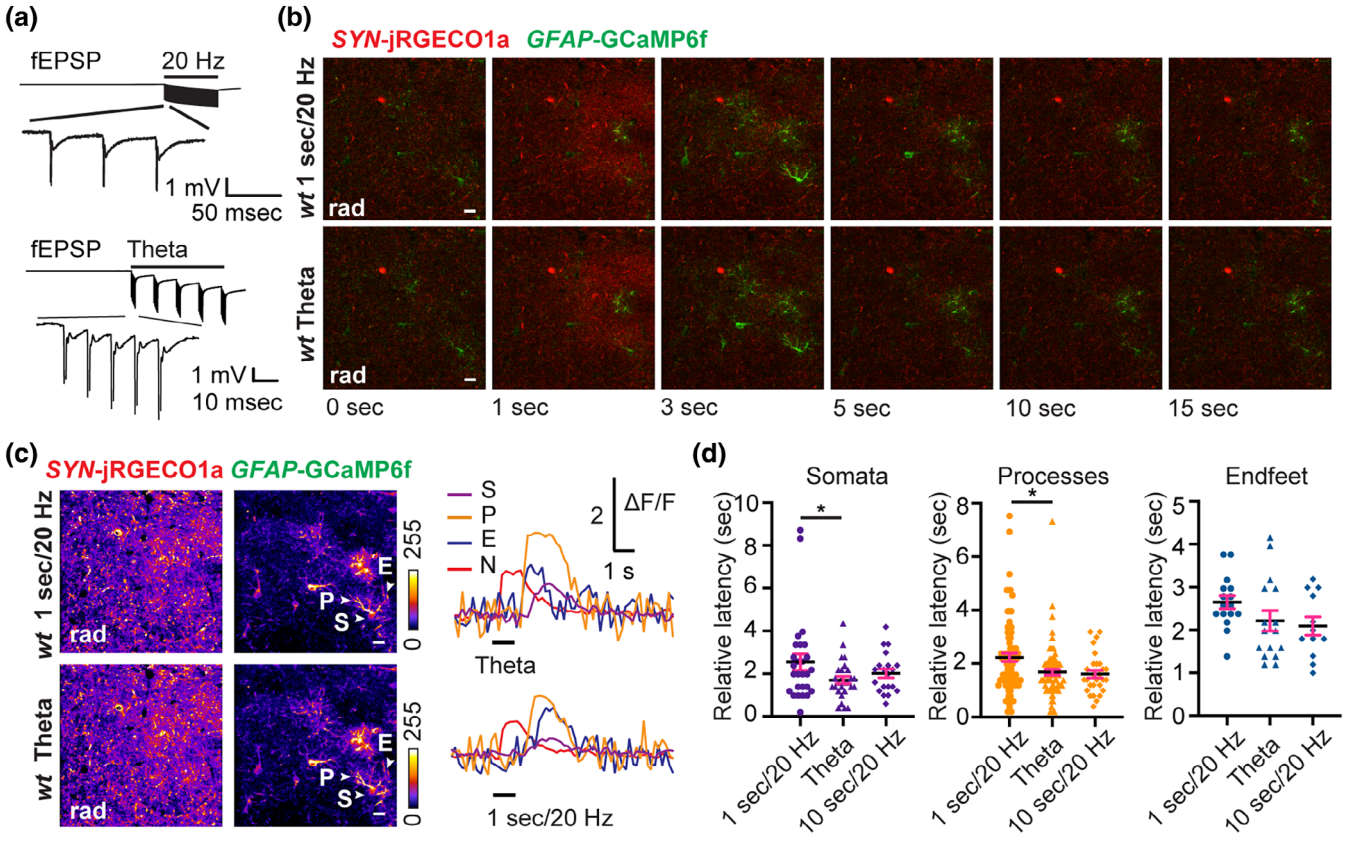

FIGURE 2 Dual-indicator two-photon imaging of Ca^{2+} elevation in acute wild-type mouse hippocampal slices transduced with rAAV-*SYN*-jRGECO1a and rAAV-*GFAP*-GCaMP6f. (a) Representative traces of fEPSP (expanded in bottom trace) recorded during 20 Hz for 1 sec (top) and theta burst (bottom) stimulation. (b) Representative time series of *GFAP*-GCaMP6f (green) and *SYN*-jRGECO1a (red) fluorescence images with two stimulation protocols of the Scc. (c) Left, standard deviation (SD) images of jRGECO1a and GCaMP6f fluorescence intensities from a time series recording with above mentioned two stimulation protocols; right, representative traces of the neuronal (N) and astrocytic (somata [S], processes [P] and endfeet [E]) Ca^{2+} signals with two stimulation protocols. (d) Latency between the onset of the neuronal jRGECO1a fluorescence transients and the onset of astrocytic GCaMP6f fluorescence transients (relative latency) in somata (left), processes (middle) and endfeet (right) with all three Scc stimulation protocols. Relative latency comparison of 20 Hz for 1 sec and theta burst ($p_{somata} = .0172$, $n = 27$; $p_{processes} = .0002$, $n = 79$; $p_{endfeet} = .0634$, $n = 16$). Relative latency comparision of theta burst and 20 Hz for 10 sec ($p_{somata} = .1579$, $n_{theta\ burst} = 27$, $n_{20\ Hz\ for\ 10\ sec} = 20$; $p_{processes} = .8723$, $n_{theta\ burst} = 79$, $n_{20\ Hz\ for\ 10\ sec} = 28$; $p_{endfeet} = .9362$, $n_{theta\ burst} = 16$, $n_{20\ Hz\ for\ 10\ sec} = 12$). Asterisks show values that differ significantly from each other. Pink bars indicate the standard error mean. Scale bar, 10 μm.

10 sec stimulation period. Taken together, the greater level of presynaptic released glutamate accelerates local astrocytic Ca^{2+} elevation.

3.3 | Direct blockage of glutamate transporters does not abolish astrocytic Ca^{2+} elevation

Since extracellular glutamate is mainly taken by glutamate transporters on astrocytic membranes, we investigated whether neuronal released glutamate through these glutamate transporters is the main cause of astrocytic Ca^{2+} elevation, we blocked glutamate transporters with their specific inhibitor DL-threo-β-benzyloxyaspartic acid (DL-TBOA, 100 μm). To obtain comparable results from our previous study (Tang et al., 2015), we continued all following experiments with neuronal stimulation protocol of 20 Hz for 10 sec. A severe reduction of fEPSP about 75% (Figure 3a) was observed, which most likely is due to the excitotoxicity of blocking glutamate transporters in neurons by DL-TBOA. Despite this severe reduction of neuronal fEPSP, the peak amplitude (Max-$\Delta F/F$) and the response duration of astrocytic Ca^{2+} elevation during 20 Hz for 10 sec Scc stimulation remained high (Figure 3b,c). Interestingly, the astrocytic response latency was significantly shortened in somata (Figure 3d), and the response rise time (time to the first peak) was significantly decreased in both somata and processes (Figure 3e). Unlike what we have expected, the blockage of glutamate transporters on astrocytes did not abolish their Ca^{2+} responses but altered their kinetics. This demonstrated that astrocytic glutamate transporters are not the direct cause of the astrocytic Ca^{2+} elevation, and that the responsible triggering mechanisms of astrocytic Ca^{2+} elevation might be indirectly associated with astrocytic glutamate uptake.

3.4 | Extracellular Ca^{2+} entry via the NCX reverse mode drives astrocytic Ca^{2+} elevation after neuronal activity

Previous studies have reported that synaptic stimulation depolarizes astrocytic membrane, and that this depolarization may be caused by the Na^+ influx through glutamate transporters and the postsynaptic K^+ efflux during repolarization (Armbruster et al., 2022; Barros et al., 2023; Bellot-Saez et al., 2017; Kirischuk et al., 2012; Pannasch et al., 2012; Rose & Karus, 2013b; Srivastava et al., 2020; Verkhratsky et al., 2020). Small elevation in astrocytic intracellular Na^+ (about 3–5-mM) and depolarized membrane potential can switch the NCX to its reverse mode (Rose et al., 2020). In the above experiment, when blocking glutamate transporters by DL-TBOA, the accumulated extracellular glutamate could cause more K^+ efflux from the postsynaptic neurons. The higher level of extracellular K^+ may act alone to depolarize the astrocytic membrane and even accelerate the process of astrocytic responses instead of the Na^+ influx through glutamate transporters as shown above (Figure 3d,e). Thus, this astrocytic membrane depolarization caused by the postsynaptic K^+ efflux with the presence of DL-TBOA may activate the reverse mode of astrocytic NCX mediating extracellular Ca^{2+} entry. Next, we asked whether blocking this Ca^{2+} influx via the NCX reverse mode would influence astrocytic Ca^{2+} elevation. A potent and selective inhibitor of NCX reverse mode, KB-R7943, was applied. Indeed, with comparable

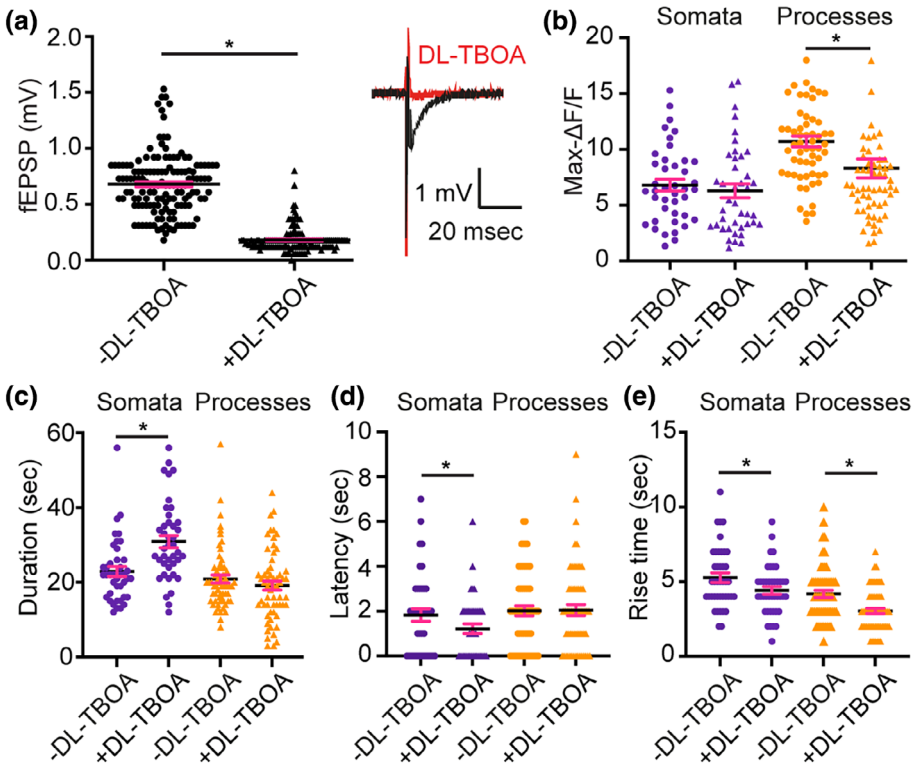

FIGURE 3 Direct blockage of glutamate transporters by DL-TBOA. (a) Quantification of neuronal fEPSPs before and after DL-TBOA wash (left, $p < .0001$, $n = 140$ from seven slices) and representative traces (right). (b) After the DL-TBOA application, the maximum $\Delta F/F$ values dropped significantly in the processes ($p = .0020$, $n = 60$). (c) The rise time decreased significantly in both soma and processes ($p_{soma} = .0171$, $n = 41$, $p_{processes} < .0001$, $n = 60$). (d) The activation duration was increased in the soma after DL-TBOA wash in ($p < .0001$, $n = 41$) whereas in the processes it was not significantly changed ($p = .1498$, $n = 60$).

neuronal stimulation strength revealed by jRGECO1a signals before and after bath application of KB-R7943 (20 μM), the astrocytic Ca^{2+} elevation was greatly attenuated in all astrocytic compartments. Particularly in somata and processes, both $\Delta F/F$ and the regions of activity (ROA, active fractions) within individual marked regions of interest (ROIs) were significantly reduced (Figure 4a–c, middle panels, Figure S1A,B). The responsive rates in active ROIs of all compartments were also dropped (Figure 4d middle panel).

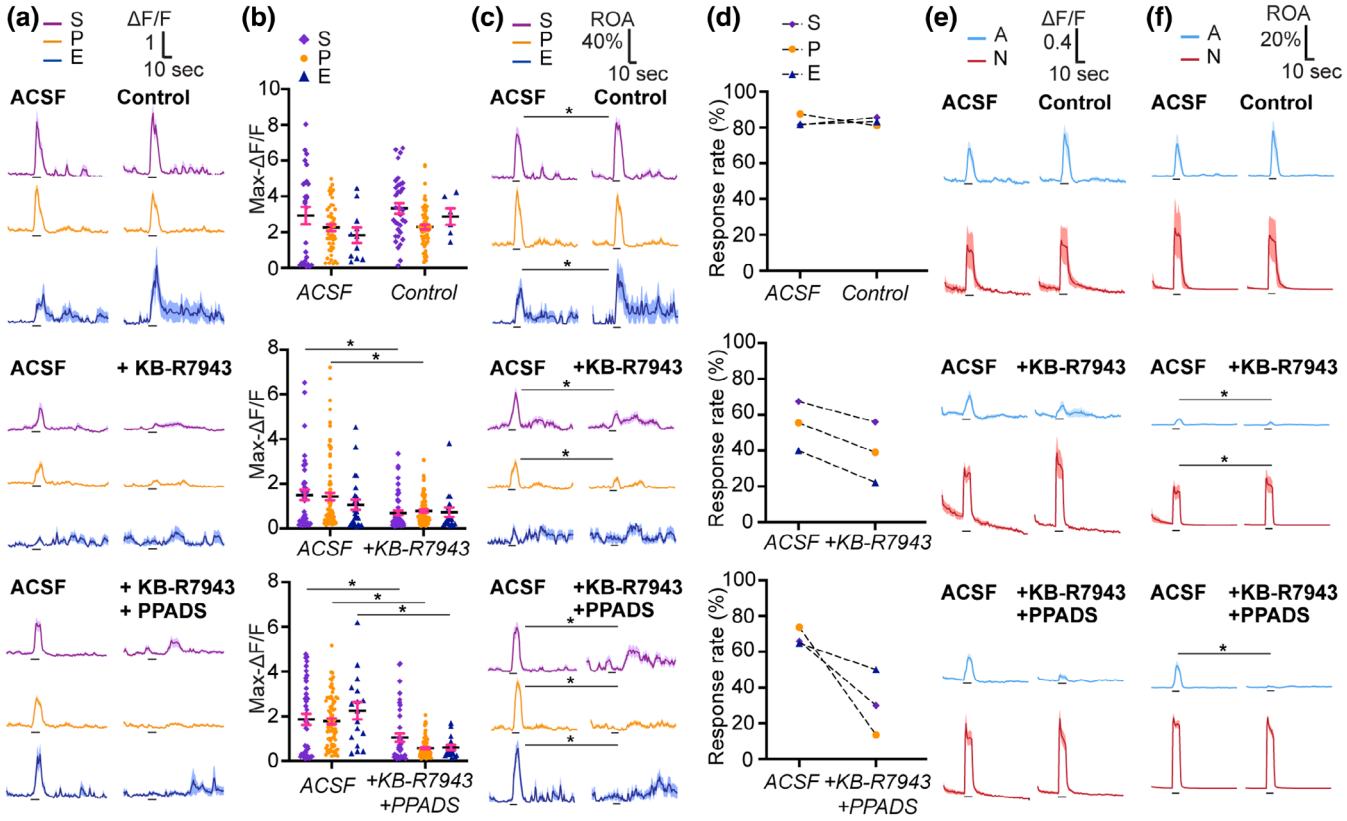

FIGURE 4 Increased astrocytic membrane Ca^{2+} permeability via NCX and P2XRs is essential for triggering neuronal-evoked astrocytic Ca^{2+} responses. (a) Average traces of *GFAP*-GCaMP6f fluorescence changes ($\Delta F/F$) from all three astrocytic compartments (Somata [S], Processes [P] and Endfeet [E]) during neuronal stimulation (indicated with bar) at 20 Hz for 10 sec. Colored shades indicate the range of standard error mean traces from all marked ROIs. Top panel, ACSF control without drug treatment; middle panel, without and with KB-R7943 treatment; bottom panel, without and with both KB-R7943 and PPADS treatment. (b) Quantification of maximum amplitude ($\Delta F/F$) of the GCaMP6f fluorescence increase in astrocytic compartments stimulated at 20 Hz for 10 sec. Top panel, ACSF control without drug treatment, two-way ANOVA, $p_{treatment} = .1208$, $F_{treatment}(1, 184) = 2.429$, $p_{compartments} = .0031$, $F_{compartments}(2, 184) = 5.973$; middle panel, without and with KB-R7943 treatment, two-way ANOVA, $p_{treatment} = .0001$, $F_{treatment}(1, 320) = 14.81$; bottom panel, without and with both KB-R7943 and PPADS treatment, two-way ANOVA, $p_{treatment} < .0001$, $F_{treatment}(1, 265) = 57.84$. (c) Average traces of active fraction in *GFAP*-GCaMP6f fluorescence changes in astrocytic ROIs (ROA in ROIs). Two-way ANOVA was performed with values in 30 sec durations after the neuronal stimulation. Top panel, ACSF control without drug treatment, $p_{Somata\text{-}treatment\text{-}ACSF} < .0001$, $F_{Somata\text{-}treatment\text{-}ACSF}(1, 1860) = 17.01$, $p_{Processes\text{-}treatment\text{-}ACSF} = .5088$, $F_{Processes\text{-}treatment\text{-}ACSF}(1, 3379) = 0.4365$, $p_{Endfeet\text{-}treatment\text{-}ACSF} = .0002$, $F_{Endfeet\text{-}treatment\text{-}ACSF}(1, 465) = 14.06$; middle panel, without and with KB-R7943 treatment, $p_{Somata\text{-}treatment\text{-}KB} = .0002$, $F_{Somata\text{-}treatment\text{-}KB}(1, 2821) = 13.80$, $p_{Processes\text{-}treatment\text{-}KB} < .0001$, $F_{Processes\text{-}treatment\text{-}KB}(1, 5828) = 104.8$, $p_{Endfeet\text{-}treatment\text{-}KB} = .0822$, $F_{Endfeet\text{-}treatment\text{-}KB}(1, 1271) = 3.026$; bottom panel, without and with both KB-R7943 and PPADS treatment, $p_{Somata\text{-}treatment\text{-}KB + PPADS} < .0001$, $F_{Somata\text{-}treatment\text{-}KB + PPADS}(1, 2449) = 38.13$, $p_{Processes\text{-}treatment\text{-}KB + PPADS} < .0001$, $F_{Processes\text{-}treatment\text{-}KB + PPADS}(1, 4805) = 569.9$, $p_{Endfeet\text{-}treatment\text{-}KB + PPADS} < .0001$, $F_{Endfeet\text{-}treatment\text{-}KB + PPADS}(1, 1209) = 91.47$. (d) Response rate of neuronal stimulation-evoked (20 Hz for 10 sec) GCaMP6f fluorescence responses dropped in astrocytic somata, processes and endfeet with single treatment of KB-R7943 (middle) and double treatment of KB-R7943 and PPADS (bottom), but not with ACSF control (top). (e) Average traces of *GFAP*-GCaMP6f fluorescence changes ($\Delta F/F$) from the recorded *striatum radiatum* fields. Top panel, ACSF control without drug treatment; middle panel, without and with KB-R7943 treatment; bottom panel, without and with both KB-R7943 and PPADS treatment. A, astrocytes; N, neurons. (f) Average traces of active fraction in *GFAP*-GCaMP6f fluorescence changes from the recorded *striatum radiatum* fields. Top panel, ACSF control without drug treatment; middle panel, without and with KB-R7943 treatment; bottom panel, without and with both KB-R7943 and PPADS treatment. Two-way ANOVA was performed with values in 30 sec durations after the neuronal stimulation. $p_{astrocytes\text{-}treatment\text{-}KB} = .0002$, $F_{astrocytes\text{-}treatment\text{-}KB}(1, 248) = 14.18$, $p_{neurons\text{-}treatment\text{-}KB} = .0288$, $F_{neurons\text{-}treatment\text{-}KB}(1, 248) = 4.835$; $p_{astrocytes\text{-}treatment\text{-}KB+PPADS} < .001$, $F_{astrocytes\text{-}treatment\text{-}KB + PPADS}(1, 248) = 183.09$. A, astrocytes; N, neurons. Asterisks show values that differ significantly from each other with Sidak's multiple comparison test. Pink bars indicate the standard error mean.

To avoid bias from manually marked astrocytic ROIs, both overall GCaMP6f $\Delta F/F$ and ROA within the recorded field of Scc regions were evaluated. Despite a significant increase of ROA in neurons, both the overall field $\Delta F/F$ and ROA of GCaMP6f were reduced after KB-R7943 blockage (Figure 4e,f middle panel). These results showed that by blocking the extracellular Ca^{2+} entry via the NCX reverse mode, the astrocytic internal release of Ca^{2+} from ER stores is greatly disturbed. Hence, it suggests that a Ca^{2+}-induced Ca^{2+} release mechanism is involved. In addition, we tested the same stimulation protocol (20 Hz for 10 sec) with *Itpr2*$^{-/-}$ mice. Both amplitudes of $\Delta F/F$ and the response rate of astrocytic Ca^{2+} elevation were greatly attenuated in these mice lacking the inositol triphosphate receptor type 2 (IP3R2, Figure S2A–D). Taken together, these results suggest that NCX reverse mode drives the IP3R2 dependent Ca^{2+}-induced Ca^{2+} release in astrocytes after neuronal glutamate release.

3.5 | Extracellular Ca^{2+} entry via purinergic P2XRs further contributes to astrocytic Ca^{2+} elevation after neuronal activity

However, when we repeated the same 20 Hz for 10 sec protocol with more intense neuronal stimulation strength that elicited population spikes, astrocytic Ca^{2+} elevation occurred once again despite the presence of KB-R7943. We then asked whether other pathways of Ca^{2+} entry like the NCX reverse mode would elicit astrocytic Ca^{2+} elevation. Besides glutamate, ATP is known as another important neurotransmitter released at excitatory synapses (Burnstock & Verkhratsky, 2012; Pankratov et al., 2006). In our previous studies we have separately examined the effect of blocking a wide range of P2 purinergic receptors with a mixture of pyridoxalphosphate-6-azophenyl-2′,4′-disulfonic acid tetrasodium salt (PPADS, 100 μM) and suramin (100 μM). And we observed reduction of astrocytic Ca^{2+} elevation about 20%–30% in astrocytic fine processes and somata, indicating that P2 purinergic receptors partially contribute to elicit Ca^{2+} elevation in astrocytes (Tang et al., 2015). In theory, the binding of ATP to purinergic P2X receptor channels (P2XRs) can lead to extracellular Ca^{2+} entry, which may also initiate Ca^{2+}-induced Ca^{2+} release in astrocytes. It has been reported that strong neuronal stimulation with high frequency can cause rapid extracellular increase of ATP released from presynaptic terminals (Wieraszko et al., 1989; Zhang et al., 2007). By blocking both the NCX reverse mode and P2XRs simultaneously with a mixture of KB-R7943 (20 μM) and PPADS (100 μM, a non-selective P2 purinergic antagonist) we experimentally approached this option. During this double blockage, despite the increased neuronal stimulation strength measured by the jRGECO1a fluorescence (Figure 4e bottom panel), astrocytic Ca^{2+} elevation in all astrocytic compartments were almost completely abolished when measuring both $\Delta F/F$ and ROA within individual marked ROIs (Figure 4a–c bottom panels, Figure S1C,D). The responsive rate of active ROIs was greatly reduced in all compartments (Figure 4d bottom panel). Both the field $\Delta F/F$ and ROA recorded in Scc regions were abolished after this double blockage (Figure 4e,f bottom panels).

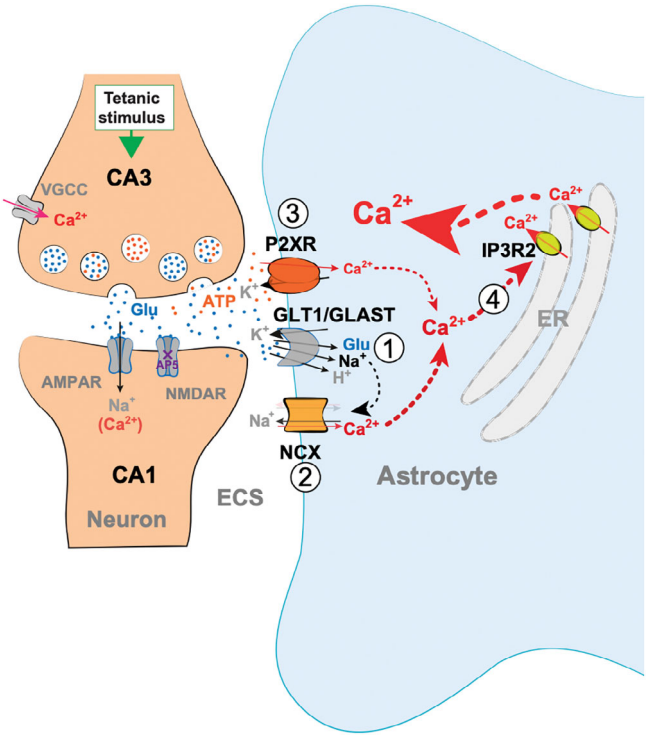

FIGURE 5 Astrocytic membrane Ca^{2+} permeability through NCX and P2X receptors governs Ca^{2+}-induced Ca^{2+} release through IP3R2 upon Scc neuronal activity. (1) The neuronal released glutamate (Glu) binds to glutamate transporters (GLT1/GLAST) on astrocytic membranes, and this causes a rapid Na^+ influx to the astrocytes. (2) The elevated intracellular Na^+ concentration in astrocytes and the depolarization of astrocytic membranes by the efflux of K^+ from postsynaptic neurons change the NCX from its forward mode (translucent arrows) to the reverse mode (solid arrows), and thus importing Ca^{2+} into astrocytes. (3) In addition, the neuronal released ATP binds to astrocytic P2X receptors and directly leads to Ca^{2+} entry into astrocytes. (4) Together, the extracellular Ca^{2+} entry via NCX reverse mode and P2X receptors facilitates the Ca^{2+}-induced Ca^{2+} release through IP3R2 on astrocytic ER. This points to a new mechanism that increases of astrocytic membrane Ca^{2+} permeability drive the neuronal evoked astrocytic Ca^{2+} elevation at CA3-CA1 Scc excitatory synapses of adult mice.

Washing in (for 1 hour) of only artificial cerebrospinal fluid (ACSF) as controls did not change levels of astrocytic Ca^{2+} elevation (Figure 4a–c,e,f top panels) as well as responsive rate of active ROIs (Figure 4d top panel). These results showed that the double blockage of the NCX reverse mode and P2X receptors abolishes Ca^{2+} elevation in astrocytes after Scc stimulation. In addition to the NCX reverse mode, the extracellular Ca^{2+} entry via P2X receptors further contributes to astrocytic Ca^{2+} elevation after neuronal activity.

Thus, the above pharmacological experiments indicate that the extracellular Ca^{2+} entry is a key driving force to elicit astrocytic Ca^{2+} elevation at electrically stimulated Scc synapses. Both NCX reverse mode and P2X receptors on astrocytic membrane are important to mediate increases of membrane Ca^{2+} permeability via neuronal released signals. These findings point to a new mechanism that increases of astrocytic membrane Ca^{2+} permeability drive the

neuronal evoked astrocytic Ca^{2+} elevation at CA3-CA1 Scc excitatory synapses of adult mice.

4 | DISCUSSION

In our previous study, we showed that stimulation evoked Ca^{2+} elevation in astrocytes at CA3-CA1 synapses of adult mice are modulated by glutamate and ATP (Tang et al., 2015). In this present follow-up study, we used traditional pharmacological and genetic approaches to identify two key membrane transporter proteins related to neuronal released glutamate and ATP, the NCX and P2X receptors which represent two important Ca^{2+} influx pathways of astrocytes. Once they are activated, the astrocytic membrane Ca^{2+} permeability is increased, allowing an IP3R2 dependent Ca^{2+}-induced Ca^{2+} release in astrocytes (Figure 5). This modulation of astrocytic membrane Ca^{2+} permeability via extracellular ions and neurotransmitters plays an important role in triggering the neuronal evoked astrocytic activity.

When we characterized presynaptic glutamate releases using iGluSnFR driven by *hSYN* promoter, the kinetics of the sensor was considered. Since the decay time of iGluSnFR is about 180 msec (Marvin et al., 2013), the area under curve of iGluSnFR signal from the 20 Hz for 1 sec stimulation cannot be counted as the total amount of glutamate released during 1 sec period. However, the florescent signal from five trains of theta burst, which has 200 msec in between each train, may reveal better the total amount of glutamate released. Since astrocytic Ca^{2+} elevation happens after about 1.7 –2 sec, both theta burst and 20 Hz for 1 sec protocols will allow the observation of potential astrocytic glutamate releases after neuronal stimulation. surprisingly, we did not detect any extracellular glutamate increases after the stimulation period (Figure 1e,g). This may be due to the sensitivity of iGluSnFR, which is not high enough to pick the astrocytic glutamate release.

In this study, we found that the astrocytic response latency during 20 Hz for 10 sec stimulation was about 2 sec (Figure 2d and Figure 3d). This agrees with our previous study on measuring the extracellular K^+ concentration ($[K^+]_o$) during 20 Hz for 10 sec Scc stimulation using potassium-sensitive electrodes (Haj-Yasein et al., 2011). Furthermore, during the strong theta burst stimulation eliciting higher level of glutamate release, more K^+ efflux may rise $[K^+]_o$ faster due to greater depolarization of postsynaptic neurons that might be reflected by the shortened astrocytic response latency down to 1.7 sec (Figure 2d). This might indicate a potential correlation between the astrocytic response latency and the $[K^+]_o$ fast rising phase. When glutamate transporters were blocked by DL-TBOA, the accumulated extracellular glutamate will greatly depolarize postsynaptic neurons. Meanwhile, the excessive K^+ efflux would also result a shorter $[K^+]_o$ fast rising phase, which could be monitored by the accelerated astrocytic responses as measured by the shortened response latency in somata and shortened rise time in both somata and processes (Figure 3d,e). Thus, the $[K^+]_o$ fast rising phase might contribute either alone or together with glutamate transporters to depolarize astrocytic membranes and active the NCX reverse mode.

The effect of the NCX blocker KB-R7943, when used at concentrations up to 30 μM, can selectively block the reverse mode of the NCX, and has little effect on other proteins, such as the Na^+–Ca^{2+}–K^+ exchanger, the Na^+, K^+-ATPase (NKA), plasma membrane Ca^{2+}-ATPase (PMCA) and sarcoendoplasmic reticulum Ca^{2+}-ATPase (SERCA), and the Na^+–H^+ exchanger (Amran et al., 2003; Iwamoto et al., 1996). Thus, the concentration of KB-R7943 used in the present study, 20 μM, can effectively block the reverse mode of the NCX without effecting above mentioned proteins in both neurons and astrocytes. It is still controversial whether KB-R7943 inhibits the mitochondrial Ca^{2+} uptake (Brustovetsky et al., 2011; Namekata et al., 2020; Santo-Domingo et al., 2007; Storozhevykh et al., 2010; Wiczer et al., 2014) in cultured neurons and other cell types. Although during our experiments, we have not observed any abnormal Ca^{2+} activity in jRGECO1a expressing neurons, to rule out the possible off-target of KB-R7943 on mitochondria, further assessment of neuronal and astrocytic mitochondrial function shall be considered, for instance, using mitochondria tagged GECIs in neurons and astrocytes to access the functionality during the Scc stimulation with the presence of KB-R7943. In rat hippocampal neurons, controversial results have also been reported on the effect of KB-R7943 on the *N*-methyl-D-aspartate receptors (NMDARs), with two IC50s of 0.8 and 11 μM (Hoyt et al., 1998; Sobolevsky & Khodorov, 1999). In astrocytes of rodents, NMDARs have a reduced Ca^{2+} permeability, which is most likely due to the relative overrepresentation of the tri-heteromeric (GluN1 + GluN2 + GluN3) configuration of NMDAR subunits in astrocytes (Henson et al., 2010; Lalo et al., 2006). In addition, it has been reported that in cultured astrocytes, NMDARs have likewise been observed to act through the non-canonical, metabotropic signaling pathways, which does not involve the membrane Ca^{2+} influx (Kondoh et al., 2001; Nishizaki et al., 1999). In our experimental settings, the activity-dependent Ca^{2+} influx of all NMDARs, including the potential astrocytic NMDARs, were blocked by 2-amino-5-phosphonovaleric acid (APV). And they could not contribute to the increasing of membrane Ca^{2+} permeability.

Both neurons and astrocytes can release ATP. We propose that the neuronal stimulation-dependent presynaptic ATP release is responsible for the activation of P2X receptors triggering astrocytic Ca^{2+} responses, since ATP releases from astrocytes occur after their Ca^{2+} elevation (Pryazhnikov & Khiroug, 2008). It is unclear whether ATP is co-released with glutamate from same presynaptic vesicles, or it is released from a separate vesicle pool at Scc excitatory synapses (Burnstock & Verkhratsky, 2012; Pankratov et al., 2006). However, previous studies show that strong neuronal stimulation with high frequency can cause rapid increase of ATP released from presynaptic terminals (Wieraszko et al., 1989; Zhang et al., 2007), indicating the likelihood that ATP from separate vesicles was released. If this separate ATP vesicle pool exists, when a higher intensity stimulation eliciting population spikes was applied, more vesicles will be release from presynaptic terminals, and ATP released from the separate vesicle pool could rapidly bind to P2X receptors mediating Ca^{2+} entry in astrocytes. Meanwhile, the stronger stimulation may also still cause more K^+ efflux from postsynaptic neurons mediating depolarization of astrocytic membrane, indicating this depolarization and reversal of NCX is not the only mechanism related to Ca^{2+} entry that can cause astrocytic Ca^{2+} rise.

In this study, we could show that increases of membrane Ca^{2+} permeability via the NCX reverse mode and P2X receptors are of primary importance to drive Ca^{2+} elevation in astrocytes at excitatory synapses. However, other mechanisms related to local neuronal activation may also contribute to astrocytic Ca^{2+} responses, such as various G protein-coupled signaling pathways. Previously, we have demonstrated that the blockage of group I/II metabotropic glutamate receptors and the P2 purinergic receptors caused reduction of the Ca^{2+} elevation in hippocampal astrocytic in adult mice (Tang et al., 2015). It has also been reported that activation of cannabinoid type-1 (CB1) receptors triggered hippocampal astrocytic Ca^{2+} elevation and modulated synaptic transmission and memory in mice (Navarrete & Araque, 2008, 2010; Robin et al., 2018). Furthermore, activation of $GABA_B$ receptors via gamma-aminobutyric acid (GABA) in mouse hippocampal and cortical astrocytes could induce astrocytic internal releases of Ca^{2+} (Mariotti et al., 2016; Perea et al., 2016). Interestingly, previous studies in rat hippocampal slices and other brain regions in mice, such as olfactory bulb, retina and cerebellum, have shown that extracellular Ca^{2+} entry via GABA transporters or Ca^{2+} permeable AMPA receptors are causes to induce astrocytic Ca^{2+} elevation upon local neuronal stimulation (Boddum et al., 2016; Doengi et al., 2009; Saab et al., 2012; Zhang et al., 2019). These data support our conclusion on the importance of astrocytic membrane Ca^{2+} permeability in general. Our results are pointing to that increases of the astrocytic membrane Ca^{2+} permeability could be the primary driving force of the Ca^{2+} elevation in astrocytes after local neuronal activity. This Ca^{2+} influx mechanism is distinct from other astrocytic activation pathways, such as neuromodulatory activation, which involves G protein-coupled receptors. Further studies in various brain regions and neuronal circuits are needed to confirm that this mechanism of increasing astrocytic membrane Ca^{2+} permeability is the essential initiation of astrocytic internal release of Ca^{2+} upon local neuronal activation.

AUTHOR CONTRIBUTIONS

Wannan Tang, Erlend A. Nagelhus, Vidar Jensen: Conceptualization and experimental design. Jarand B. Hjukse, Mario F. D. L. Puebla, Gry Fluge Vindedal, Rolf Sprengel, Vidar Jensen, Wannan Tang: Experimental conduct and methodology. Wannan Tang: Writing. Wannan Tang and Erlend A. Nagelhus: Funding.

ACKNOWLEDGMENTS

We thank Prof. Loren L. Looger for providing all genetically encoded sensors, and Johannes Helm for technical support on the two-photon microscopy.

FUNDING INFORMATION

This work was supported by the Research Council of Norway with grant number 262552, HELSE MIDT-NORGE with grant number 28293, Felles forskningsutvalg (FFU) with grant number 34226, the European Union's Seventh Framework Programme for research, technological development and demonstration under grant number 601055, and the Letten Foundation.

CONFLICT OF INTEREST STATEMENT

The authors declare no conflict of interest.

DATA AVAILABILITY STATEMENT

The original recorded data are available upon requests. The analysis tools have been shared on Github.

ORCID

Erlend A. Nagelhus https://orcid.org/0000-0002-8090-4362

Wannan Tang https://orcid.org/0000-0002-2263-6435

REFERENCES

Amran, M. S., Homma, N., & Hashimoto, K. (2003). Pharmacology of KB-R7943: A Na^+–Ca^{2+} exchange inhibitor. *Cardiovascular Drug Reviews*, *21*(4), 255–276.

Armbruster, M., Naskar, S., Garcia, J. P., Sommer, M., Kim, E., Adam, Y., Haydon, P. G., Boyden, E. S., Cohen, A. E., & Dulla, C. G. (2022). Neuronal activity drives pathway-specific depolarization of peripheral astrocyte processes. *Nature Neuroscience*, *25*, 607–616.

Barros, L. F., Ruminot, I., Sotelo-Hitschfeld, T., Lerchundi, R., & Fernández-Moncada, I. (2023). Metabolic recruitment in brain tissue. *Annual Review of Physiology*, *85*, 115–135.

Bazargani, N., & Attwell, D. (2016). Astrocyte calcium signaling: The third wave. *Nature Neuroscience*, *19*, 182–189. https://doi.org/10.1038/nn.4201

Bellot-Saez, A., Kékesi, O., Morley, J. W., & Buskila, Y. (2017). Astrocytic modulation of neuronal excitability through K^+ spatial buffering. *Neuroscience & Biobehavioral Reviews*, *77*, 87–97. https://doi.org/10.1016/j.neubiorev.2017.03.002

Bennay, M., Langer, J., Meier, S. D., Kafitz, K. W., & Rose, C. R. (2008). Sodium signals in cerebellar Purkinje neurons and Bergmann glial cells evoked by glutamatergic synaptic transmission. *Glia*, *56*, 1138–1149.

Bergles, D. E., & Jahr, C. E. (1998). Glial contribution to glutamate uptake at Schaffer collateral-commissural synapses in the hippocampus. *The Journal of Neuroscience*, *18*, 7709–7716.

Bjørnstad, D. M., Åbjørsbråten, K. S., Hennestad, E., Cunen, C., Hermansen, G. H., Bojarskaite, L., Pettersen, K. H., Vervaeke, K., & Enger, R. (2021). Begonia—A two-photon imaging analysis pipeline for astrocytic Ca^{2+} signals. *Frontiers in Cellular Neuroscience*, *15*, 1–12.

Boddum, K., Jensen, T. P., Magloire, V., Kristiansen, U., Rusakov, D. A., Pavlov, I., & Walker, M. C. (2016). Astrocytic GABA transporter activity modulates excitatory neurotransmission. *Nature Communications*, *7*, 13572.

Bondarenko, A., Svichar, N., & Chesler, M. (2005). Role of Na^+-H^+ and Na^+-Ca^{2+} exchange in hypoxia-related acute astrocyte death. *Glia*, *49*, 143–152.

Bowser, D. N., & Khakh, B. S. (2004). ATP excites interneurons and astrocytes to increase synaptic inhibition in neuronal networks. *The Journal of Neuroscience*, *24*, 8606–8620.

Brustovetsky, T., Brittain, M. K., Sheets, P. L., Cummins, T. R., Pinelis, V., & Brustovetsky, N. (2011). KB-R7943, an inhibitor of the reverse Na^+/Ca^{2+} exchanger, blocks N-methyl-D-aspartate receptor and inhibits mitochondrial complex i. *British Journal of Pharmacology*, *162*, 255–270.

Burnstock, G., & Verkhratsky, A. (2012). Purinergic signalling and the nervous system. In *Purinergic signalling and the nervous system* (pp. 433–581). Springer.

Chen, T. W., Wardill, T. J., Sun, Y., Pulver, S. R., Renninger, S. L., Baohan, A., Schreiter, E. R., Kerr, R. A., Orger, M. B., Jayaraman, V., Looger, L. L., Svoboda, K., & Kim, D. S. (2013). Ultrasensitive fluorescent proteins for imaging neuronal activity. *Nature*, *499*, 295–300.

Dana, H., Mohar, B., Sun, Y., Narayan, S., Gordus, A., Hasseman, J. P., Tsegaye, G., Holt, G. T., Hu, A., Walpita, D., Patel, R., Macklin, J. J., Bargmann, C. I., Ahrens, M. B., Schreiter, E. R., Jayaraman, V.,

Looger, L. L., Svoboda, K., & Kim, D. S. (2016). Sensitive red protein calcium indicators for imaging neural activity. *eLife*, *5*, e12727.

Deitmer, J. W., & Rose, C. R. (2010). Ion changes and signalling in perisynaptic glia. *Brain Research Reviews*, *63*, 113–129.

Doengi, M., Hirnet, D., Coulon, P., Pape, H. C., Deitmer, J. W., & Lohr, C. (2009). GABA uptake-dependent Ca^{2+} signaling in developing olfactory bulb astrocytes. *Proceedings of the National Academy of Sciences of the United States of America*, *106*, 17570–17575.

Droste, D., Seifert, G., Seddar, L., Jädtke, O., Steinhaüser, C., & Lohr, C. (2017). Ca2+−permeable AMPA receptors in mouse olfactory bulb astrocytes. *Scientific Reports*, *7*, 44817.

Enger, R., Tang, W., Vindedal, G. F., Jensen, V., Helm, P. J., Sprengel, R., Looger, L. L., & Nagelhus, E. A. (2015). Dynamics of ionic shifts in cortical spreading depression. *Cerebral Cortex*, *25*, 4469–4476.

Felix, L., Delekate, A., Petzold, G. C., & Rose, C. R. (2020). Sodium fluctuations in astroglia and their potential impact on astrocyte function. *Frontiers in Physiology*, *11*, 871.

Gerkau, N. J., Rakers, C., Durry, S., Petzold, G. C., & Rose, C. R. (2018). Reverse NCX attenuates cellular sodium loading in metabolically compromised cortex. *Cerebral Cortex*, *28*, 4264–4280.

Goldman, W. F., Yarowsky, P. J., Juhaszova, M., Krueger, B. K., & Blaustein, M. P. (1994). Sodium/calcium exchange in rat cortical astrocytes. *The Journal of Neuroscience*, *14*, 5834–5843.

Haj-Yasein, N. N., Jensen, V., Vindedal, G. F., Gundersen, G. A., Klungland, A., Ottersen, O. P., Hvalby, Ø., & Nagelhus, E. A. (2011). Evidence that compromised K^+ spatial buffering contributes to the epileptogenic effect of mutations in the human kir4.1 gene (KCNJ10). *Glia*, *59*, 1635–1642.

Henson, M. A., Roberts, A. C., Pérez-Otaño, I., & Philpot, B. D. (2010). Influence of the NR3A subunit on NMDA receptor functions. *Progress in Neurobiology*, *91*, 23–37.

Hirrlinger, J., Scheller, A., Hirrlinger, P. G., Kellert, B., Tang, W., Wehr, M. C., Goebbels, S., Reichenbach, A., Sprengel, R., Rossner, M., & Kirchhoff, F. (2009). Split-Cre complementation indicates coincident activity of different genes in vivo. *PLoS One*, *4*, e4286.

Hoyt, K. R., Arden, S. R., Aizenman, E., & Reynolds, I. J. (1998). Reverse Na^+/Ca^{2+} exchange contributes to glutamate-induced intracellular Ca^{2+} concentration increases in cultured rat forebrain neurons. *Molecular Pharmacology*, *749*, 742–749.

Iwamoto, T., Watano, T., & Shigekawa, M. (1996). A novel isothiourea derivative selectively inhibits the reverse mode of Na^+/Ca^{2+} exchange in cells expressing NCX1. *Journal of Biological Chemistry*, *271*, 22391–22397. https://doi.org/10.1074/jbc.271.37.22391

King, C. M., Bohmbach, K., Minge, D., Delekate, A., Zheng, K., Reynolds, J., Rakers, C., Zeug, A., Petzold, G. C., Rusakov, D. A., & Henneberger, C. (2020). Local resting Ca^{2+} controls the scale of Astroglial Ca^{2+} signals. *Cell Reports*, *30*, 3466–3477.

Kirischuk, S., Kettenmann, H., & Verkhratsky, A. (1997). Na^+/Ca^{2+} exchanger modulates kainate-triggered Ca^{2+} signaling in Bergmann glial cells in situ. *The FASEB Journal*, *11*, 566–572.

Kirischuk, S., Kettenmann, H., & Verkhratsky, A. (2007). Membrane currents and cytoplasmic sodium transients generated by glutamate transport in Bergmann glial cells. *Pflügers Archiv-European Journal of Physiology*, *454*, 245–252.

Kirischuk, S., Parpura, V., & Verkhratsky, A. (2012). Sodium dynamics: Another key to astroglial excitability? *Trends in Neurosciences*, *35*, 497–506.

Kondoh, T., Nishizaki, T., Aihara, H., & Tamaki, N. (2001). NMDA-responsible, APV-insensitive receptor in cultured human astrocytes. *Life Sciences*, *68*, 1761–1767.

Lalo, U., Pankratov, Y., Kirchhoff, F., North, R. A., & Verkhratsky, A. (2006). NMDA receptors mediate neuron-to-glia signaling in mouse cortical astrocytes. *The Journal of Neuroscience*, *26*, 2673–2683.

Langer, J., & Rose, C. R. (2009). Synaptically induced sodium signals in hippocampal astrocytes in situ. *The Journal of Physiology*, *587*, 5859–5877.

Li, X., Zima, A. V., Sheikh, F., Blatter, L. A., & Chen, J. (2005). Endothelin-1-induced arrhythmogenic Ca^{2+} signaling is abolished in atrial myocytes of inositol-1,4,5-trisphosphate(IP3)-receptor type 2-deficient mice. *Circulation Research*, *96*, 1274–1281.

Mariotti, L., Losi, G., Sessolo, M., Marcon, I., & Carmignoto, G. (2016). The inhibitory neurotransmitter GABA evokes long-lasting Ca^{2+} oscillations in cortical astrocytes. *Glia*, *64*, 363–373.

Marvin, J. S., Borghuis, B. G., Tian, L., Cichon, J., Harnett, M. T., Akerboom, J., Gordus, A., Renninger, S. L., Chen, T. W., Bargmann, C. I., Orger, M. B., Schreiter, E. R., Demb, J. B., Gan, W. B., Hires, S. A., & Looger, L. L. (2013). An optimized fluorescent probe for visualizing glutamate neurotransmission. *Nature Methods*, *10*, 162–170.

Namekata, I., Odaka, R., Hamaguchi, S., & Tanaka, H. (2020). KB-R7943 inhibits the mitochondrial Ca^{2+} uniporter but not Na^+–Ca^{2+} exchanger in cardiomyocyte-derived H9c2 cells. *Biological & Pharmaceutical Bulletin*, *43*, 1993–1996.

Navarrete, M., & Araque, A. (2008). Endocannabinoids mediate neuron-astrocyte communication. *Neuron*, *57*, 883–893.

Navarrete, M., & Araque, A. (2010). Endocannabinoids potentiate synaptic transmission through stimulation of astrocytes. *Neuron*, *68*, 113–126. https://doi.org/10.1016/j.neuron.2010.08.043

Nishizaki, T., Matsuoka, T., Nomura, T., Kondoh, T., Tamaki, N., & Okada, Y. (1999). Store Ca^{2+} depletion enhances NMDA responses in cultured human astrocytes. *Biochemical and Biophysical Research Communications*, *259*, 661–664.

Pankratov, Y., Lalo, U., Verkhratsky, A., & North, R. A. (2006). Vesicular release of ATP at central synapses. *Pflügers Archiv-European Journal of Physiology*, *452*, 589–597.

Pannasch, U., Sibille, J., & Rouach, N. (2012). Dual electrophysiological recordings of synaptically-evoked astroglial and neuronal responses in acute hippocampal slices. *Journal of Visualized Experiments*, *69*, e4418.

Perea, G., Gómez, R., Mederos, S., Covelo, A., Ballesteros, J. J., Schlosser, L., Hernández-Vivanco, A., Martín-Fernández, M., Quintana, R., Rayan, A., Díez, A., Fuenzalida, M., Agarwal, A., Bergles, D. E., Bettler, B., Manahan-Vaughan, D., Martín, E. D., Kirchhoff, F., & Araque, A. (2016). Activity-dependent switch of gabaergic inhibition into glutamatergic excitation in astrocyte-neuron networks. *eLife*, *5*, 1–26.

Porter, J. T., & McCarthy, K. D. (1996). Hippocampal astrocytes in situ respond to glutamate released from synaptic terminals. *The Journal of Neuroscience*, *16*, 5073–5081.

Pryazhnikov, E., & Khiroug, L. (2008). Sub-micromolar increase in $[Ca^{2+}]i$ triggers delayed exocytosis of ATP in cultured astrocytes. *Glia*, *56*, 38–49.

Robin, L. M., Oliveira da Cruz, J. F., Langlais, V. C., Martin-Fernandez, M., Metna-Laurent, M., Busquets-Garcia, A., Bellocchio, L., Soria-Gomez, E., Papouin, T., Varilh, M., Sherwood, M. W., Belluomo, I., Balcells, G., Matias, I., Bosier, B., Drago, F., van Eeckhaut, A., Smolders, I., Georges, F., … Marsicano, G. (2018). Astroglial CB1 receptors determine synaptic D-serine availability to enable recognition memory. *Neuron*, *98*, 935–944.

Rojas, H., Colina, C., Ramos, M., Benaim, G., Jaffe, E. H., Caputo, C., & DiPolo, R. (2007). Na^+ entry via glutamate transporter activates the reverse Na^+/Ca^{2+} exchange and triggers Cai^{2+}-induced Ca^{2+} release in rat cerebellar Type-1 astrocytes. *Journal of Neurochemistry*, *100*, 1188–1202.

Rose, C. R., & Karus, C. (2013a). Two sides of the same coin: Sodium homeostasis and signaling in astrocytes under physiological and pathophysiological conditions. *Glia*, *61*, 1191–1205.

Rose, C. R., & Karus, C. (2013b). *Two sides of the same coin: Sodium homeostasis and signaling in astrocytes under physiological and pathophysiological conditions*. Glia.

Rose, C. R., & Verkhratsky, A. (2016). Principles of sodium homeostasis and sodium signalling in astroglia. *Glia*, *64*, 1611–1627.

Rose, C. R., Ziemens, D., & Verkhratsky, A. (2020). On the special role of NCX in astrocytes: Translating Na^+-transients into intracellular Ca^{2+} signals. *Cell Calcium*, *86*, 102154. https://doi.org/10.1016/j.ceca.2019.102154

Saab, A. S., Neumeyer, A., Jahn, H. M., Cupido, A., Šimek, A. A. M., Boele, H. J., Scheller, A., Le Meur, K., Götz, M., Monyer, H., Sprengel, R., Rubio, M. E., Deitmer, J. W., De Zeeuw, C. I., & Kirchhoff, F. (2012). Bergmann glial AMPA receptors are required for fine motor coordination. *Science*, *337*, 749–753.

Santello, M., Toni, N., & Volterra, A. (2019). Astrocyte function from information processing to cognition and cognitive impairment. *Nature Neuroscience*, *22*, 154–166.

Santo-Domingo, J., Vay, L., Hernández-SanMiguel, E., Lobatón, C. D., Moreno, A., Montero, M., & Alvarez, J. (2007). The plasma membrane Na^+/Ca^{2+} exchange inhibitor KB-R7943 is also a potent inhibitor of the mitochondrial Ca^{2+} uniporter. *British Journal of Pharmacology*, *151*, 647–654.

Shevtsova, Z., Malik, J. M. I., Michel, U., Bähr, M., & Kügler, S. (2005). Promoters and serotypes: Targeting of adeno-associated virus vectors for gene transfer in the rat central nervous system in vitro and in vivo. *Experimental Physiology*, *90*, 53–59.

Shigetomi, E., Kracun, S., Sofroniew, M. V., & Khakh, B. S. (2010). A genetically targeted optical sensor to monitor calcium signals in astrocyte processes. *Nature Neuroscience*, *13*, 759–766.

Smith, R. H., Levy, J. R., & Kotin, R. M. (2009). A simplified baculovirus-AAV expression vector system coupled with one-step affinity purification yields high-titer rAAV stocks from insect cells. *Molecular Therapy*, *17*, 1888–1896. https://doi.org/10.1038/mt.2009.128

Sobolevsky, A. I., & Khodorov, B. I. (1999). Blockade of NMDA channels in acutely isolated rat hippocampal neurons by the Na^+/Ca^{2+} exchange inhibitor KB-R7943. *Neuropharmacology*, *38*, 1235–1242.

Srivastava, I., Vazquez-Juarez, E., & Lindskog, M. (2020). Reducing glutamate uptake in rat hippocampal slices enhances astrocytic membrane depolarization while Down-regulating CA3–CA1 synaptic response. *Frontiers in Synaptic Neuroscience*, *12*, 1–11.

Storozhevykh, T. P., Senilova, Y. E., Brustovetsky, T., Pinelis, V. G., & Brustovetsky, N. (2010). Neuroprotective effect of KB-r7943 against glutamate excitotoxicity is related to mild mitochondrial depolarization. *Neurochemical Research*, *35*, 323–335.

Tang, W., Szokol, K., Jensen, V., Enger, R., Trivedi, C. A., Hvalby, Ø., Johannes Helm, P., Looger, L. L., Sprengel, R., & Nagelhus, E. A. (2015). Stimulation-evoked Ca^{2+} signals in astrocytic processes at hippocampal CA3-CA1 synapses of adult mice are modulated by glutamate and ATP. *The Journal of Neuroscience*, *35*, 3016–3021.

Verkhratsky, A., Untiet, V., & Rose, C. R. (2020). Ionic signalling in astroglia beyond calcium. *The Journal of Physiology*, *598*, 1655–1670.

Wiczer, B. M., Marcu, R., & Hawkins, B. J. (2014). KB-R7943, a plasma membrane Na^+/Ca^{2+} exchanger inhibitor, blocks opening of the mitochondrial permeability transition pore. *Biochemical and Biophysical Research Communications*, *444*, 44–49. https://doi.org/10.1016/j.bbrc.2014.01.009

Wieraszko, A., Goldsmith, G., & Seyfried, T. N. (1989). Stimulation-dependent release of adenosine triphosphate from hippocampal slices. *Brain Research*, *485*, 244–250.

Zhang, R., Du, W., Prober, D. A., & Du, J. (2019). Müller glial cells participate in retinal waves via glutamate transporters and AMPA receptors. *Cell Reports*, *27*, 2871–2880.

Zhang, X., Chen, Y., Wang, C., & Huang, L. Y. M. (2007). Neuronal somatic ATP release triggers neuron-satellite glial cell communication in dorsal root ganglia. *Proceedings of the National Academy of Sciences of the United States of America*, *104*, 9864–9869.

SUPPORTING INFORMATION

Additional supporting information can be found online in the Supporting Information section at the end of this article.

How to cite this article: Hjukse, J. B., Puebla, M. F. D. L., Vindedal, G. F., Sprengel, R., Jensen, V., Nagelhus, E. A., & Tang, W. (2023). Increased membrane Ca^{2+} permeability drives astrocytic Ca^{2+} dynamics during neuronal stimulation at excitatory synapses. *Glia*, *71*(12), 2770–2781. https://doi.org/10.1002/glia.24450